





Correlation of structural and magnetic properties of $R\text{FeO}_3$ ($R = \text{Dy}, \text{Lu}$)

Banani Biswas,¹ Pavel Naumov,^{1,2} Federico Motti,^{1,3} Patrick Hautle¹,,¹ Marek Bartkowiak¹,,¹
Ekaterina V. Pomjakushina,¹ Uwe Stuhr,¹ Dirk Fuchs,⁴ Thomas Lippert^{1,5},,^{1,5} and Christof W. Schneider^{1,*},

¹Paul Scherrer Institute, 5232 Villigen PSI, Switzerland

²Orange Quantum System B.V., Elektronicaweg 2, 2628 XG Delft, The Netherlands

³Istituto Officina dei Materiali - CNR-IOM, 34149 Basovizza (Trieste), Italy

⁴Karlsruhe Institute of Technology, Institute for Quantum Materials and Technologies, Kaiserstr. 12, 76131 Karlsruhe, Germany

⁵Department of Chemistry and Applied Biosciences, Laboratory of Inorganic Chemistry, ETH Zurich, Switzerland



(Received 24 March 2024; accepted 25 July 2024; published 9 August 2024)

In orthoferrites the rare-earth (R) ion has a big impact on structural and magnetic properties; in particular, the ionic size influences the octahedral tilt and the R^{3+} - Fe^{3+} interaction modifies properties like the spin reorientation. Growth-induced strain in thin films is another means to modify materials properties since the sign of strain affects the bond length and therefore directly the orbital interaction. Our study focuses on epitaxially grown (010)-oriented DyFeO_3 and LuFeO_3 thin films, thereby investigating the impact of compressive lattice strain on the magnetically active Dy^{3+} and magnetically inactive Lu^{3+} compared to uniaxially strained single-crystal DyFeO_3 . The DyFeO_3 films exhibit a shift of more than 20 K in spin-reorientation temperatures, maintain the antiferromagnetic Γ_4 phase of the Fe lattice below the spin reorientation, and show double-step hysteresis loops for both in-plane directions between 5 and 390 K. This is the signature of an Fe-spin-induced ferromagnetic Dy^{3+} lattice above the Néel temperature of the Dy. The observed shift in the film spin reorientation temperatures vs lattice strain is in good agreement with isostatic single-crystal neutron diffraction experiments with a rate of 2 K/kbar.

DOI: [10.1103/PhysRevMaterials.8.084404](https://doi.org/10.1103/PhysRevMaterials.8.084404)

I. INTRODUCTION

The orthorhombic perovskite $R\text{FeO}_3$ (orthoferrites; R , rare earth) is an interesting and technically relevant class of materials for spintronics applications, and has been investigated extensively since the 1960s [1]. Their distinct magnetic properties such as high Néel temperatures ($T_N > 600$ K), a canted antiferromagnetic (AFM) G-type spin structure, a spin reorientation transition (SRT) whose value depends strongly on the ionic size of the rare-earth (R) element, and an ordering of the rare-earth ions at low temperatures are also very attractive to study their basic magnetic properties [1,2]. Some of the $R\text{FeO}_3$ compounds also show ferroelectric (FE) properties [2–4]. Recently, this class of materials gained attention through studies of their low-temperature magnetic field properties [5–7] and the prediction that uniaxial stress will induce FE behavior even well above room temperature, potentially with a large electrical polarization [8,9]. Such a room-temperature multiferroic state would have potential applications in spin-based electronic devices.

Strain or externally applied pressure can alter mechanical, chemical, electrical, and magnetic properties of a material [10]. Chemical pressure in which an atom is replaced by another atom is the typical means to introduce strain in a crystalline structure [11–13]. Examples are among the rare-earth manganites where the decrease in ionic radius leads to a distortion of the ideal cubic structure. The lattice responds to the mismatch of the R -O and Mn-O equilibrium bond lengths by changing the rotation of the MnO_6 octahedra. As a consequence the antiferromagnetic ground state shifts from an A-type to a spin spiral and finally arrives at an E-type AFM state [14]. This is also reflected in the stability of the crystalline structure, where the stable structure will change from orthorhombic to hexagonal with decreasing ionic radius [14]. In thin films epitaxial strain provides control over materials properties by adopting appropriately growth conditions and lattice mismatch between substrate and films to arrive at designed materials properties [15–20]. Chemically induced strain is more closely related to the three-dimensional (3D) structure of a material, whereas epitaxial strain is more of a two-dimensional (2D) type often paired with anisotropic strain characteristics depending on the crystalline symmetry of the substrate and film.

DyFeO_3 is one member of the $R\text{FeO}_3$ family with the space group $Pbnm$ and known to show magnetic-ordering-driven multiferroic properties below 4 K [4,6,21]. The two magnetic ions form two separate spin lattices and their interaction gives rise to Fe^{3+} - Fe^{3+} , Dy^{3+} - Fe^{3+} , and Dy^{3+} - Dy^{3+} exchange interactions, which dominate at different temperature regimes.

*Contact author: christof.schneider@psi.ch

Published by the American Physical Society under the terms of the Creative Commons Attribution 4.0 International license. Further distribution of this work must maintain attribution to the author(s) and the published article's title, journal citation, and DOI.

The strong $\text{Fe}^{3+}\text{-Fe}^{3+}$ interaction results in a G-type AFM ordering along the a axis and the Dzyaloshinskii-Moriya (DM) interaction in a tilting of the oxygen octahedra along the c axis. As a consequence, there is a weak ferromagnetic (wFM) component and A-type AFM ordering below the Néel temperature of the Fe lattice ($T_{\text{N,Fe}} = 645$ K). The interaction between Dy and Fe ($\text{Dy}^{3+}\text{-Fe}^{3+}$) becomes more relevant with decreasing temperature, which eventually leads to a spin reorientation (SR) in the Fe lattice at around 50 K. As a result, the expected Curie-Weiss temperature dependence is changed near T_{SR} , and below the G-type AFM ordering switches from the a to the b direction. This is unlike LuFeO_3 , which is a single-spin AFM system with no SR. The change in spin direction for DyFeO_3 goes hand in hand with a change in the spin configuration represented as $G_x A_y F_z$ or Γ_4 phase to the spin state below T_{SR} represented as $A_x G_y C_z$ or Γ_1 phase [2]. $G_x A_y$ is associated with a magnetic 222 symmetry of the crystal and $A_x G_y$ with an $mm2$ symmetry. At around 4 K Dy ordering takes place and the spins align antiferromagnetically in the ab plane [6]. Applying a magnetic field below $T_{\text{N,Dy}}$ larger than ~ 2.3 T along the c axis [4], the Fe lattice switches back from the Γ_1 phase to the more stable Γ_4 phase. Parallel with the change in symmetry a displacement of the Dy atoms along [001] in the unit cell takes place. This magnetic-field-induced displacement results in a polar unit cell giving rise to FE behavior below $T_{\text{N,Dy}}$. As pointed out in Ref. [3], applying uniaxial pressure along [110] below $T_{\text{N,Dy}}$ reduces the magnetic point group symmetry 222 down to 2 since two mirror planes are removed. As a consequence, a FE polarization is introduced below $T_{\text{N,Dy}}$ with the ferromagnetic (FM) moment parallel to [001] [3].

In this paper, we study the effect of growth-induced strain on the magnetic properties of the nominally multiferroic materials DyFeO_3 and LuFeO_3 as thin films by growing them epitaxially strained on (010)-oriented YAIO_3 substrates with a compressive in-plane strain. For the magnetic characterization, the temperature dependence of the magnetic moment (M) was measured along the magnetic soft axis [001] for DyFeO_3 to investigate the strain dependence of the spin reorientation as well as the moment vs magnetic field ($M(H)$) up to 7 T between 1.8 and 390 K for both materials and all three main crystallographic axes. To compare the effect of compressive strain and pressure on the magnetic thin-film properties, neutron diffraction measurements were performed to probe the temperature dependence of the SR of a DyFeO_3 single crystal in a He gas pressure cell with an isostatic pressure up to 4 kbar (0.4 GPa). The hydrostatic pressure conditions and orientation-dependent neutron diffraction measurements allow to draw parallels to orientation-dependent magnetic thin-film measurements, thereby taking into account the anisotropic stress states of coherently grown films.

II. EXPERIMENTAL METHODS

Epitaxial thin films of DyFeO_3 ($a = 5.302$ Å, $b = 5.598$ Å, and $c = 7.623$ Å) and LuFeO_3 ($a = 5.2176$ Å, $b = 5.5556$ Å, and $c = 7.5749$ Å) are grown on (010)-oriented YAIO_3 single crystalline substrates ($a = 5.18$ Å, $b = 5.330$ Å, and $c = 7.375$ Å) by pulsed laser deposition using a KrF

excimer laser ($\lambda = 248$ nm, 3 Hz) with an in-plane lattice mismatch between (010) DyFeO_3 and a (010) YAIO_3 substrate of -2.36% along the a axis, -3.36% along the c axis, and -5.03% along the b axis [22]. The lattice mismatch for LuFeO_3 is -0.73% along the a axis, -4.23% along the b axis, and -2.71% along the c axis. YAIO_3 is a nonmagnetic and nonferroelectric insulating substrate and therefore suitable to study magnetic and dielectric or FE properties of multiferroic films on the same substrate. The laser beam is focused onto a sintered ceramic target with a spot size of 1.4×1.4 mm² with the laser fluence adjusted to 2.0 J cm⁻². The substrate is located on axis to the plasma plume with a distance of 5 cm from the target. Deposition was performed in an O_2 background at 0.33 mbar with the substrate heated to 700 °C by a lamp heater [22]. Five films of different thickness have been deposited subsequently (13, 27, 51, 78, and 115 nm) to study the thickness dependence of crystalline and magnetic properties. Other films discussed were prepared at different preparation runs with the aforementioned deposition conditions.

The structural quality of the powder and single crystal and the thickness of the films after the deposition have been monitored by x-ray diffraction (XRD) and x-ray reflection (XRR), respectively, using a Seifert 3003 PTS and a Bruker D8 Advance four-circle x-ray diffractometer with a $\text{Cu } K\alpha_1$ monochromatic x-ray source. Θ - 2Θ scans have been used to monitor the crystalline quality of all samples, reciprocal space maps to determine in-plane lattice constants and to evaluate qualitatively strain in these films, and XRR to determine the thickness of the films after the deposition.

The temperature-dependent magnetization was investigated by a commercially available superconducting quantum interference device (SQUID) magnetometer (Quantum Design, MPMS^R 3). It enables temperature sweeps between 1.8 and 400 K with a magnetic field of up to 7 T parallel to the measurement direction. The evolution of the magnetic moment (M) with temperature has been analyzed by the following measurement protocol. First, the sample is cooled down without applied field to 3 K. The zero-field cooling (ZFC) $M(T)$ measurement is taken during heating between 3 and 300 K in the presence of a small field applied along the measurement direction. After each measurement cycle, the film was kept at 390 K for 5 min to erase as much as possible trapped fields. Normally, the annealing temperature should be higher than $T_{\text{N,bulk}} \sim 645$ K. Due to instrumental limitations, the maximum temperature which can be reached inside the SQUID is ~ 400 K. However, this temperature is not enough to remove trapped stray fields inside the film completely; increasing the temperature up to ~ 400 K will certainly increase thermal fluctuations of the magnetic spin and minimize trapped fields since T_{N} for strained films is expected to be considerably lower than $T_{\text{N,bulk}}$ [6]. This procedure provided reproducible nominal ZFC $M(T)$ measurements even after measuring $M(H)$ up to 7 T. After this annealing process, the samples are cooled down with an applied field and measurements are taken during cooling [field-cooled cooling (FCC)] and heating [field-cooled heating (FCH)].

Neutron diffraction studies were performed at the spallation neutron source SINQ, Paul Scherrer Institute (Villigen, Switzerland). Single-crystal neutron diffraction experiments

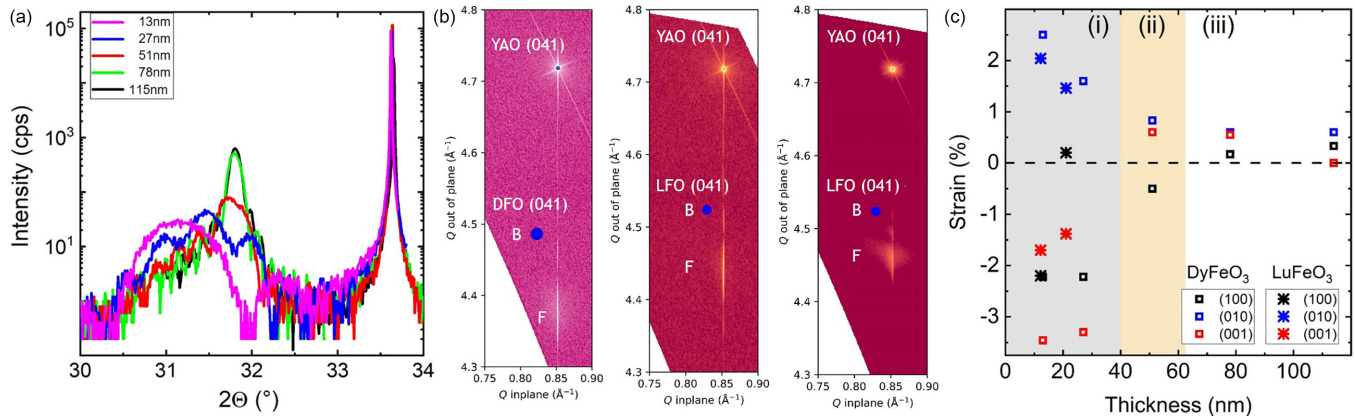


FIG. 1. (a) Θ - 2Θ measurement of the (020) DyFeO₃ and (020) YAO substrate Bragg peak for films of different thickness. (b) Reciprocal space maps of the (041) reflections of a 13-nm (010) DyFeO₃ film, and 11.6-nm and 21-nm (010) LuFeO₃ films grown on (010) YAlO₃. The blue dot in each map indicates the expected position of bulk DyFeO₃ or LuFeO₃. The bulk position is labeled B, the film position with F. (c) Crystalline-axis-dependent strain vs film thickness for (010) DyFeO₃ and LuFeO₃ grown on (010) YAlO₃.

were conducted at the thermal triple-axis spectrometer EIGER with $k_f = 2.66 \text{ \AA}^{-1}$ ($\lambda = 2.36 \text{ \AA}$) [23] using a pyrolytic graphite filter to eliminate higher-order neutrons. The zero-field experiments were done in a He cryostat to reach temperatures down to 1.5 K with the sample mounted in the (0 kl) scattering plane. For the pressure-dependent measurements, a helium gas pressure cell [24–26] has been used with a maximum reachable pressure of 5 kbar to study the spin re-orientation transition at 40 K in a single crystal under uniaxial pressure conditions between 1.5 and 100 K. In the temperature regime of interest, the gas-pressure cell has the advantage that the pressure medium He is in the gas phase or liquid and the applied pressure is therefore truly isostatic. This enables to understand orientation-dependent measurements correctly. At temperatures below 20 K, He solidifies at the selected pressures and the required isostatic pressure conditions would not be fully met. The cell design is a monobloc thick-wall cylinder cell with a 16-mm-diam bore-hole similar to a design described by Aso *et al.* [24] and the He pressure is measured via a pressure gauge. To minimize neutron absorption, the aluminum alloy (Al 7049A-T6) is used to build the cells containing an active volume of $\sim 0.010l$. For the measurements, the cell is mounted on a dedicated cryostat insert inside a cryogenic system suitable to be used at the EIGER beam line. For each pressure value, a k scan was done at 80 and 5 K to determine the background contribution for the appropriate background correction and lattice constants.

III. EXPERIMENTAL RESULTS

A. Crystallographic structure of (010)-oriented DyFeO₃ and LuFeO₃ thin films

The crystalline quality of the DyFeO₃ films with five different thicknesses was studied using XRD. All films are (010) oriented and show a good crystalline quality with the FWHM for the ω scans of $\sim 0.02^\circ$ or smaller [22]. The strain for the (010) out-of-plane direction is tensile for all film thicknesses measured [Fig. 1(a)] and thickness dependent [22]. For thinner films of around 10 nm, it is of the order 2–3% and

decreases down to $< 1\%$ for films with a thickness of 100 nm or more. Films with a thickness between 15 and 20 nm grow coherent as shown, for example, in Fig. 1(b) for a 13-nm thin film with the in-plane axes aligned macroscopically with the substrate. The FWHM of the film Laue oscillations is close to the instrumental resolution (0.003°) of the diffractometer. Thicker films show a relaxation towards the bulk DyFeO₃ Bragg position, but some remnants of the initial coherent layer can still be found effectively forming a two-layered film system. Evaluating the DyFeO₃ film lattice parameters we can distinguish three regimes [(i) highly strained, (ii) strained, and (iii) largely relaxed] with a change-over in the 40-nm range of film thickness [Fig. 1(c)]. Two film thickness for LuFeO₃ have been studied: a fully coherently grown sample with 21 unit cells (11.7 nm) and one sample with 21 nm. Like for DyFeO₃, the strain in the b direction is tensile and smaller than for DyFeO₃ and the in-plane [001] strain is compressive. For the a direction, the 11.7-nm film has a compressive strain, whereas the 21-nm film is largely relaxed in this direction and lightly tensile. From the reciprocal space maps, both films look coherently grown with strain fields developing for the thicker film [Fig. 1(b)]. This also holds for the (140) Bragg peak. Interesting to note is the fact that the compressive strain along [100] for the 21-u.c. film is much larger (-2.2%) than one would expect for a nominal -0.73% substrate-bulk lattice mismatch followed by a 0.2% tensile strain for the thicker film. The reason for this finding is not fully understood.

For a thickness thinner than 40 nm, films are highly strained with a constant unit cell volume of $\sim 219 \text{ \AA}^3$, whereas films thicker than 40 nm are partially strained and the constant unit cell volume ($\sim 229 \text{ \AA}^3$) is similar to unstrained DyFeO₃ ($\sim 226 \text{ \AA}^3$). This is also reflected when calculating the out-of-plane strain, which is $\sim 2.6\%$ and $\sim 1.6\%$ for the 13- and 27-nm films, respectively, and $\sim 0.6\%$ for the thicker films. The experimental situation for the two LuFeO₃ films with respect to the unit cell volume is different. The volume of unstrained LuFeO₃ ($\sim 219.6 \text{ \AA}^3$) is smaller than the volume of the fully coherently grown LuFeO₃ film ($\sim 223.8 \text{ \AA}^3$), indicating a Poisson ratio < 0.5 .

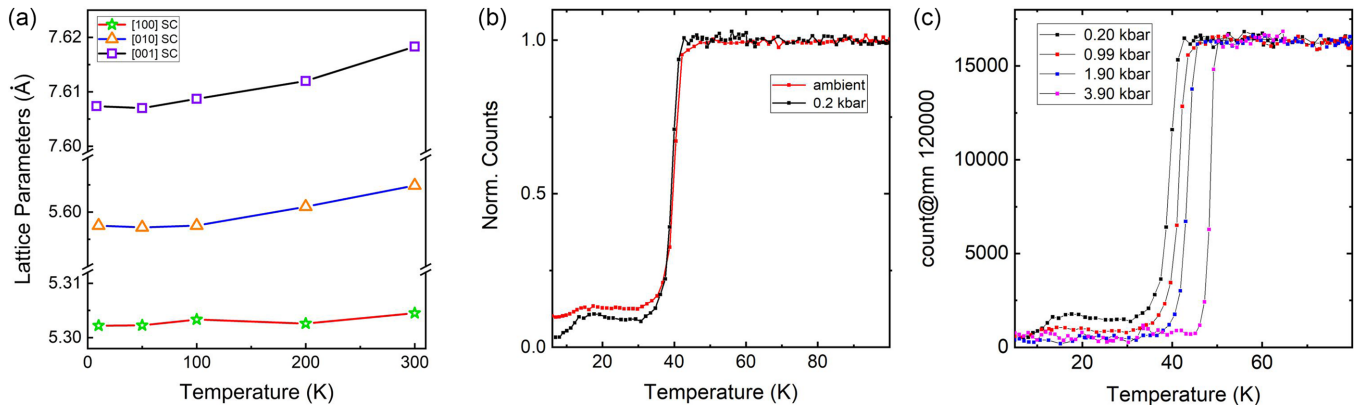


FIG. 2. (a) Temperature dependence of the DyFeO₃ single-crystal lattice constants at ambient pressure. (b) Magnetic (031) diffraction peak of a DyFeO₃ single crystal measured at ambient pressure and 0.2 kbar. (c) Pressure dependence of the magnetic (031) diffraction peak of a DyFeO₃ single crystal. The measured intensity has been recorded with a monitor of 120 000.

B. Magnetic properties

The Fe lattice in bulk DyFeO₃ orders antiferromagnetically with the spin pointing along the *a* axis. At ~ 50 K [4–6,27,28] the Fe spins reorient themselves from the *a* to the *b* direction as a consequence of the increase in the Fe³⁺-Dy³⁺ interaction and the space group changes from Γ_4 to Γ_1 . With the change in magnetic symmetry, the wFM component of Γ_4 vanishes below T_{SR} . The change and direction of the Fe spin under isostatic pressure can be verified by neutron diffraction by measuring the temperature dependence of the (031) Bragg peak of a DyFeO₃ single crystal.

1. Temperature- and isostatic-pressure-dependent single-crystal neutron diffraction

The magnetic properties of DyFeO₃ are known to be very sensitive to external stimuli due to the very small interaction energies involved [7]. This seems to be a general characteristic for the RFeO₃ family. So far, mainly magnetic-field-dependent measurements have been done, revealing strong changes in the magnetization, in particular at low magnetic fields at and below T_{SR} . Looking into the pressure dependence of the spin reorientation is therefore of interest since an applied pressure will change the bond length and therefore the interaction strength. Tensile strain, i.e., quasinegative pressure, is expected to weaken the interaction whereas compressive strain (positive pressure) should strengthen it. In the latter case, T_{SR} should increase. Isotropic pressure-dependent single-crystal neutron diffraction measurements can hence be used as a frame of reference for magnetic thin-film data in particular for the compressively in-plane strained thin films. The aim of these experiments is therefore to distinguish between pressure-induced uniaxial effects on the magnetic ions, e.g., a change in T_{SR} , and anisotropic, lattice-related effects on magnetic signatures as they potentially occur in strained thin films.

The temperature dependence of the (100), (010), and (001) lattice constants at ambient pressure conditions are shown in Fig. 2(a) as determined using the Morpheus beam line at SINQ, PSI [7]. They vary remarkably little between room temperature and 2 K. The difference for the *a* direction is 0.0023 Å, for the *b* direction 0.0074 Å, and for the *c* direction

0.011 Å. Applying a pressure up to 3.9 kbar, we measure at 8 and 100 K a pressure-induced change of the lattice parameter of 0.01 Å/kbar along [100] and 0.015 Å/kbar along [001]; the [010] direction has not been measured. The pressure-induced changes for the lattice constants are larger than the temperature-dependent changes of the lattice constants shown in Fig. 2(a). They are also larger than the changes in lattice parameter obtained from pressure-dependent Raman measurements [29].

To characterize the temperature dependence of the SR, the maximum peak intensity of the magnetic (031) Bragg peak was measured between 5 and 100 K at ambient pressure [7] and for a pressure window between 200 bars (the smallest reachable pressure in the cell) and 3.9 kbar [Figs. 2(b) and 2(c)]. For this scattering geometry, the spin propagation vector q_{Fe} is along [100] above T_{SR} and along [010] below. In Fig. 2(b), an ambient pressure measurement is compared to the 200-bar measurement. Both measurements show a constant count rate above T_{SR} , indicating that all measured moments are aligned along [100] [7] and the sharp drop at T_{SR} is unchanged with increasing pressure. Below T_{SR} the additional step in intensity between 10 and 20 K is still measurable as for the ambient pressure measurement, albeit the intensity under pressure is lower. This indicates already even a small pressure—small compared to the nominal pressure associated with a film-substrate lattice mismatch—is having a measurable effect on the spin alignment in an orthoferrite system. This observation is also in line with the sensitivity of DyFeO₃ with respect to pressure as reported in Ref. [3]. With increasing pressure, the sharpness of the SR-transition remains unchanged and the intensity below T_{SR} reaches a value associated with the background of the (031) peak at 3.9 kbar and 6 K [Fig. 2(c)]. These measurements show that the Fe spins flip almost completely from [100] to [010] at T_{SR} and the increase of T_{SR} with pressure takes place at a rate of 2 K/kbar (20 K/GPa). This rate is similar to measurements performed on hematite where a rate of 3 K/kbar on T_{SR} in a hydrostatic environment up to 0.6 GPa was reported [30,31]. However, measurements in a nonhydrostatic environment up to 10 GPa showed a change in T_{SR} between 0 and 7 GPa of ~ 12 K and deviatoric stress was mentioned as a likely reason for this very different pressure-dependent behavior.

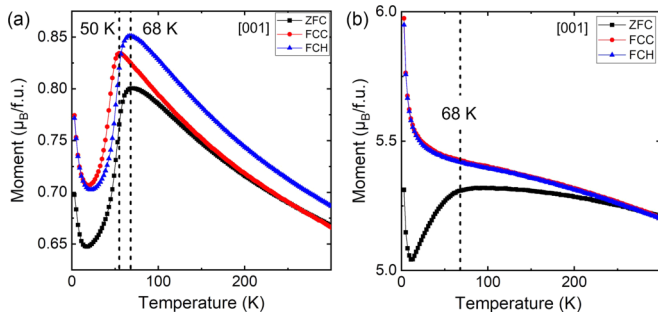


FIG. 3. (a) ZFC and FC measurements of a 115-nm, (010)-oriented DyFeO_3 thin film along [001] with a magnetic field of $H = 0.1$ T. The dashed lines show the transition temperatures at 68 and 50 K. (b) ZFC and FC measurements of a 13-nm, (010)-oriented DyFeO_3 thin film along [001] with a magnetic field of $H = 0.1$ T. The dashed line shows the transition temperature at 68 K.

Like for an ambient pressure measurement, there is no sign of a Dy ordering along [001] at low temperatures. We therefore conclude to have a Dy ordering below 5 K in the ab plane in the presence of an isostatic pressure [7].

2. Temperature dependence of the magnetic moment in zero field for thin films

We first present zero-field cooled $M(T)$ measurements for the 115-nm-thick film between 300 and 2 K for the c -direction, the magnetic soft axis [Fig. 3(a)]. The thickest film has the most relaxed structure compared with thinner films and $M(T)$ is expected to be similar to single-crystal data. For films with thicknesses between the largest and smallest strain values the general features described next can be systematically changed between the two extremes, but details partially depend on exact preparation conditions. For a single crystal two magnetic transitions are observed, one at ~ 6 K and one at ~ 41 K, with the first one being $T_{N,\text{Dy}}$, and the latter T_{SR} where the Fe spins flip from the b into the a direction as determined from neutron diffraction measurements [7] (see Fig. S2 of the Supplemental Material [32]). Characteristic for this SRT is a width spanning only a few Kelvin within most Fe spins changing direction.

The ZFC measurement along [001] for the 115-nm film shows a Fe spin reorientation transition at ~ 68 K and at ~ 17 K a rise in the moment down to the lowest temperature measured [Fig. 3(a)]. Whereas Dy ordering is observed for the a and b directions at ~ 4.5 K, there is no signature of T_{SR} along the a and b directions at any temperature above. In analogy to a single crystal [7] there is AFM Dy ordering in the ab plane below $T_{N,\text{Dy}}$; however, the low-temperature $M(T)$ upturn along [001] is unlike known properties for a single crystal with a potential ordering temperature well below 1.6 K. For a single crystal the measured moment along [001] at T_{SR} is $\sim 0.15\mu_{\text{B}}/\text{f.u.}$; for the film it is $\sim 0.8\mu_{\text{B}}/\text{f.u.}$ and therefore considerably larger. Both values are measured with $H = 0.1$ T. At T_{SR} , the change in slope along the c axis is rather broad and occurs over a large temperature window, in stark contrast to the abrupt drop in moment for the single crystal. Assuming the direct analogy to the single crystal, the

Fe spin will point along [100] above T_{SR} and along [010] below.

$M(T)$ measurements along [001] for the highly strained 13-nm-thick film shows a change in curvature at ~ 68 K and the signal drops very slowly with decreasing temperature until at ~ 13 K the moment rises again [Fig. 3(b)]. Like for the 115-nm-thick film, the low-temperature rise in moment is taken as evidence of a starting Dy ordering with an AFM Dy ordering below 4.5 K in the ab plane and the measured moment at T_{SR} reaches $\sim 5.28\mu_{\text{B}}/\text{f.u.}$ along [001]. ZFC $M(T)$ measurements for films with thicknesses of 27, 51, and 78 nm showed similar properties as shown for the thinnest and thickest films with a Dy ordering between 4 and 5 K for [100] and [010]. The measured moments at SRT increase with decreasing thickness and values are between the thickest and thinnest films (see Fig. S1 of the Supplemental Material [32]).

3. Field-cooled thin-film measurements

Trapped fields in single crystals can have a pronounced influence on $M(T)$ resulting in additional steps and humps at temperatures typically above T_{SR} [7]. The origins of the field sensitivity are the small interaction energies, in particular along the soft magnetic axis, and T_{SR} is systematically shifted to lower temperatures with increasing field. In the case of relatively thick films (>40 nm), the onset of the transition associated with the SR for FC measurements can vary significantly. An example is shown in Fig. 3(a), where FCC and FCH for the 115-nm-thick film is shown. For the FCC measurement, T_{SR} is shifted to lower temperatures by 18 K and the value of M has increased. The same finding applies for the FCH measurement where the values for M are larger compared to the ZFC measurement and T_{SR} is back to 70 K. Likewise, the opposite can happen. Trapped fields shift T_{SR} up, in some cases even well beyond 100 K. Larger values for $M(T)$ for FC measurements is a general observation for films of all thicknesses. For films with a thickness of less than 40 nm, the SRT measured along the c direction is not measurable anymore [Fig. 3(b)].

The ZFC and FC (heating or cooling) curves along [001] show a divergence at low temperature and they converge near room temperature (~ 250 K). Besides, the net moment during any field-cooled measurement shows a higher value at a fixed temperature than the moment measured during ZFC for the temperature range below 250 K. The evolution of the interaction between the Dy and Fe lattice with applied magnetic field is a possible reason for this behavior. The magnetic interaction between Dy^{3+} and Fe^{3+} has been reported to induce ordering of the Dy lattice for single crystal DyFeO_3 at ~ 210 K along the c axis and the direction of the Dy^{3+} spins depends on the direction of the applied magnetic field [5].

Near room temperature, the Dy^{3+} spin system is the paramagnet and thermal energy prevents the ordering of the Dy lattice [5]. As the thermal fluctuations are reduced with decreasing temperature, the induced magnetic ordering of the Dy^{3+} spin lattice increases due to a dominant increase in Dy^{3+} - Dy^{3+} interaction. During the ZFC measurements, the sample is cooled down to 3 K in the absence of a field. The spin state of the Fe lattice at 3 K is in the Γ_1 phase. The

induced weak magnetic ordering of the Dy lattice is linked with the Fe lattice in the Γ_4 phase. Therefore, there is no or a small contribution from the Dy^{3+} ion to the total moment below T_{SR} . For field-cooled (FC) measurements, the absence of a SR would indicate that the Fe lattice stays in the Γ_4 phase below T_{SR} and the Dy^{3+} spin alignment is linked to Γ_4 . Therefore, the combined contribution of the Dy^{3+} and Fe^{3+} moments increases the total moment for these FC measurements, which leads to the separation between the ZFC and FC curves.

4. $M(H, T)$ and double-step hysteresis loops

Isothermal field-dependent magnetic measurements, $M(H)$, along all three major axes have been performed on these films to study the spin interactions Fe^{3+} - Fe^{3+} , Dy^{3+} - Fe^{3+} , and Dy^{3+} - Dy^{3+} between 1.8 and 390 K. For single-crystal DyFeO_3 , $M(H)$ loops along [001] show a small magnetic hysteresis at low fields and a saturation moment of $0.15\mu_B$ at 50 K with the hysteresis closing at T_{SR} . No hysteresis is observed for the other directions [7]. The closing hysteresis at T_{SR} is the signature of the change in spin direction and the change in magnetic symmetry from Γ_4 to Γ_1 . In contrast to a single crystal, a FM hysteresis for the 115-nm-thick film is observed for all three crystalline directions at room temperature [Fig. 4(a)] and also measured for all films of different thickness between 1.8 and 390 K. For examples, $M(H, T)$ along [100] for the 115-nm-thick film is shown in Fig. 4(b). It is clear that the hysteresis loops along [001] are sustained even well below T_{SR} with an increase in remanence and coercivity with decreasing temperature. Since the change from Γ_4 to Γ_1 compensates the FM contribution, the presence of a FM hysteresis loop between 1.8 and 390 K irrespective of the film's thickness.

For $M(H)$ loops measured along the in-plane [100] and [001] directions, double-step (DS) hysteresis loops are observed as shown in Fig. 4(a), and for films of different thickness [Fig. 4(c)], for example, shown at 80 K along [001]. Similar to the FM hysteresis loops, the DS hysteresis loops are observed for all film thicknesses and within a temperature range between ~ 10 and 390 K [Fig. 4(b)]. Common is also the large magnetic field (up to ~ 1 T) where the step takes place. The DS hysteresis loops were observed for the in-plane [100] and [001] directions and not for [010]. Below ~ 10 K, Dy ordering starts to take place and the DS hysteresis loops become a single hysteresis loop indicating a substantial increase in the Dy^{3+} - Dy^{3+} interaction. The origin of a DS hysteresis loop in a potential two-spin system is the coupling between two ferromagnetic layers or lattices with different coercive fields [33–37]. Measuring $M(H, T)$ for LuFeO_3 films with $m_{\text{Lu}} = 0$ and similar strain properties like DyFeO_3 , we find for the a direction of the coherently grown, 21-u.c.-thick film a DS hysteresis loop [Fig. 4(d)] and a single loop for [001] between 50 and 390 K albeit with a smaller switching field at DS compared to DyFeO_3 films. The observation of a DS hysteresis loop for this single spin system cannot originate from a coupling of spin systems but must instead arise from a change of the canting angles and a distortion of the Fe-O octahedra as a consequence of growth-induced

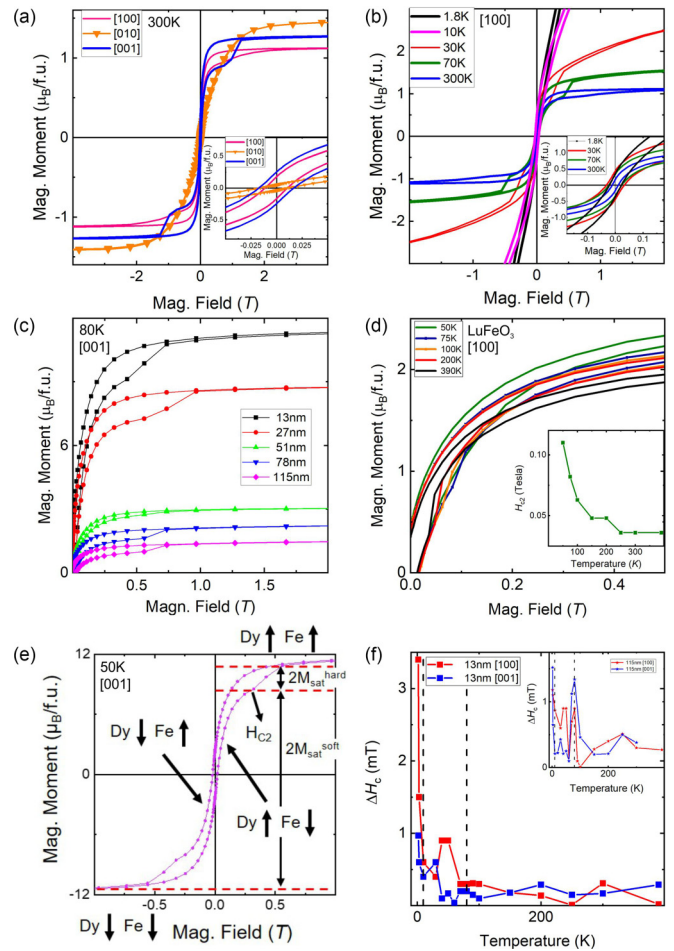


FIG. 4. (a) $M(H)$ at RT along [100], [010], and [001] for the 115-nm-thick film. Inset: FM hysteresis. (b) $M(H)$ between 300 and 1.8 K of 115-nm-thick film along [100]. (c) Double-step hysteresis along [001] at 80 K for all film thicknesses. (d) $M(H, T)$ along [100] for a 21-u.c. (010)-oriented LuFeO_3 thin film. Inset: Coercive field (H_{C2}) vs temperature. (e) Explanation of the double-step hysteresis at 50 K. The arrows show the direction of the spin alignment for the Fe and Dy magnetic lattices. $M_{\text{sat}}^{\text{hard}}$ and $M_{\text{sat}}^{\text{soft}}$ represent the saturation moment of the hard magnetic ordering (Fe) and soft magnetic ordering (Dy), respectively. H_{C2} represents the coercive field associated to the hard magnetic ordering. (f) Exchange bias field $\Delta H_c(T)$ along [100] and [001] for the 13-nm-thick film and 115-nm-thick film (inset).

compressive strain. This is equivalent to a biaxial magnetic anisotropic strain in a unit cell [38–41], here -2.2% and -1.7% for [100] and [001], respectively, giving rise to a stronger Fe-O octahedra tilting and hence a canting along both in-plane directions. Since strain values for the LuFeO_3 film are similar to DyFeO_3 , strain-induced DS hysteresis in DyFeO_3 hysteresis loops can be expected. In DyFeO_3 films, however, the DS hysteresis loops occur largely as result of a coupling between the ferromagnetically ordered Fe lattice and the induced ferromagnetically ordered Dy lattice [5] since coercive field values are considerably larger as compared to LuFeO_3 because both moments add up. Furthermore, for DyFeO_3 films the DS hysteresis loops are present for both in-plane directions, whereas for LuFeO_3 films the DS hysteresis

loops are measured only along one crystallographic direction, the [100] direction. The magnetic field H_{C2} at which the step occurs increases monotonically from 0.04 T at 390 K to 0.11 T at 50 K [Fig. 4(d), inset].

A schematic representation of the spin alignment of the Fe and Dy at different field values is illustrated in Fig. 4(e) for the [001] direction at 50 K with the arrows indicating the direction of the spin alignment for the Fe and Dy lattices. However, the spin system in our films switches from a FM-FM coupling to a FM-AFM coupling below $T_{N,Dy}$ as Dy orders antiferromagnetically in the ab plane. As a result, with the onset of Dy ordering the DS hysteresis loop vanishes and the center of the hysteresis is shifted, leading to an exchange bias effect. The applied magnetic field can change the spin alignment in the Dy spin lattice above T_{SR} from an AFM to a FM configuration. It is therefore expected to measure an exchange bias effect, particularly at low temperatures since a DyFeO₃ film seems to be a natural FM-AFM spin multilayer where a pinning of the FM with the AFM spin lattice can occur. In Fig. 4(f) the temperature dependence of the exchange bias field ΔH_c for [100] and [001] for the 13- and 115-nm-thick films is shown. Above 150 K, for both film thicknesses there is no clear exchange bias effect to be measured. This changes below 100 K. In the temperature window where the bulk SR is expected, the signals for both film thicknesses become more pronounced with a clear increase in the exchange field below 10 K, the temperature regime where Dy ordering sets in. The deviation from a standard Curie-Weiss temperature dependence below 100 K is already noticeable in Fig. 3(a) for the 115-nm-thick film and likewise apparent for the single-crystal measurements along [001] (see Fig. S2 of the Supplemental Material [32]). These changes in $M(T)$ for the single crystal are attributed to a competition between the Dy and Fe spins, and hence the Dy³⁺-Fe³⁺ interaction leading to the SR. For films the magnetic situation is similar and the Fe spins partially compensate for the FM Dy component while going through a SR, however, without changing the magnetic symmetry. To yield a more pronounced exchange bias at higher temperatures the magnetic anisotropy needs to be enhanced to clamp the magnetization sufficiently. Consequently, the LuFeO₃ films with the nonmagnetic Lu do not display any exchange bias, the measured moments are clearly smaller than for DyFeO₃ films, and H_{C2} is almost a factor of 10 smaller due to the absence of a Lu³⁺-Lu³⁺ interaction.

5. Magnetic exchange fields

To evaluate the ordering of the spin systems, the saturation moment for the 13-nm-thick film at 50 K for both spin systems (hard and soft) is measured, which are $\sim 1.445\mu_B$ and $\sim 9.875\mu_B$, respectively, and the maximum moments Fe³⁺ and Dy³⁺ can reach are $5.91\mu_B$ and $10.6\mu_B$, respectively [Fig 5(d)]. Therefore, the soft magnetic ordering in DyFeO₃ films originates from the ordering of the Dy lattice. The soft magnetic ordering is also orientation and thickness dependent [Figs. 5(a) and 5(b)]. Measuring $M_{sat}^{soft}(T)$ for [100] and [001] for the 115- and 13-nm-thick films [Fig. 5(c)], it is clear that for the 13-nm-thick film [100] is the dominant direction, whereas for the 115-nm-thick film both directions are almost equal as one would expect it to be for a single crystal. A

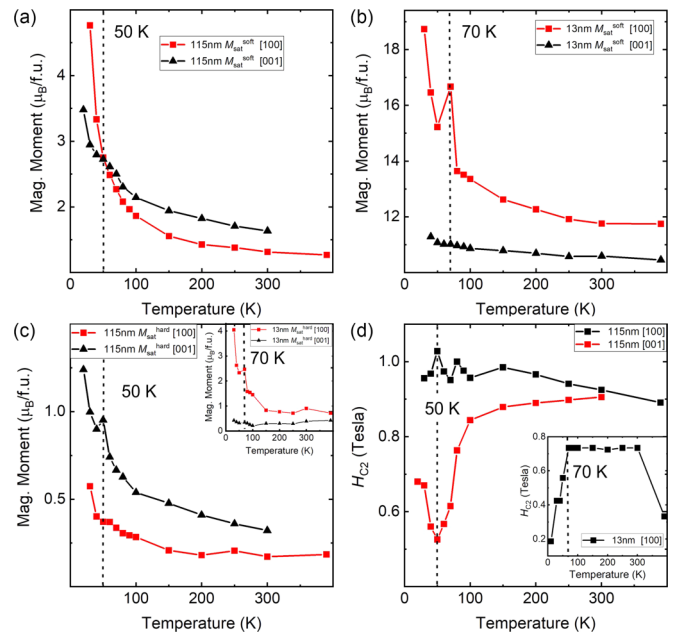


FIG. 5. (a) M_{sat}^{soft} vs T of a 115-nm-thick DyFeO₃ film along [100] and [001]. (b) M_{sat}^{soft} vs T of a 13-nm-thick DyFeO₃ film along [100] and [001]. (c) M_{sat}^{hard} vs T of a 115-nm-thick film along [100] and [001]. Inset: M_{sat}^{hard} vs T of a 13-nm-thick film along [100] and [001]. (d) H_{C2} vs T of a 115-nm-thick film along [100] and [001]. Inset: H_{C2} vs T of a 13-nm-thick film along [100].

likely explanation is the large difference in growth-induced strain in the 13-nm-thick film giving rise to the anisotropy for the moments as well as large differences in the absolute values for μ_B . The smaller values for the thick film are closer to values measured for single crystals [7]. In Figs. 5(a) and 5(b) the dashed line at 50 K indicates where a maximum or a plateau for the soft component appears. Comparing these measurements to the $M(T)$ measurements shown in Fig. 3, we note that transition temperatures identified at ~ 70 K are related to the Fe spin reorientation, whereas the signature at ~ 50 K is directly linked to Dy and hence the Dy³⁺-Fe³⁺ interaction. It is worth mentioning that the constant presence of the DS hysteresis loops at all measurable temperatures indicates the influence of Dy at room temperature and above. Besides, the large M_{sat}^{soft} component in thinner films at room temperature shows that in highly strained films the influence of the Dy³⁺ spins is more dominant as compared to thicker films.

So far, we have shown that the magnetic properties of strained DyFeO₃ thin films are orientation dependent and the Dy³⁺-Fe³⁺ interaction is noticeable up to 390 K. Unlike in a DyFeO₃ single crystal, Dy³⁺ is magnetically active along [100] and [001] in the entire temperature window above and below $T_{N,Dy}$. This is evident when measuring $H_{C2}(T)$ for the 13- and 115-nm-thick thin films [Fig. 5(d)]. The coercive field H_{C2} for the [100] direction is almost temperature independent and just below 1 T for the 115-nm-thick film. For the [001] direction, it is smaller and has a distinct minimum at around T_{SR} indicating that the Fe lattice undergoes a partial SR. However, the value of H_{C2} partially recovers with further decreasing temperature. The coercive field H_{C2}

is also considerably smaller than the critical field needed to induce ferroelectricity in bulk. The situation is similar for the 13-nm-thick film. Between 300 and 70 K $H_{C2}(T)$ is temperature independent along [100] and starts to drop when SR occurs. Below 70 K it is not possible to determine H_{C2} . For the [001] direction, no data can be extracted from $M(H)$ loops as the measured hysteresis cannot be clearly distinguished from a DS hysteresis and a potential value for H_{C2} would be similar to the maximum applied field of 5 T used to measure $M(H)$. However, for the other film thicknesses investigated, the tendency was as shown exemplary for the thinnest and thickest films. The meaning of the identified extrema at 60 K for [001] and at 50 and 80 K for [100] is not clear at present. These measurements show that [100] is the magnetically distinct and dominant direction with respect to the Dy^{3+} - Fe^{3+} interaction as compared to [001] even well above room temperature. For single crystals no DS hysteresis loops are measured for any crystalline direction in the temperature regime between room temperature and 10 K [7]. A possible explanation for the stronger influence of the Dy^{3+} along [100] can be the result of the orbital overlap of the Dy^{3+} with the oxygen in the unit cell due to the mixture of compressive and tensile strain.

IV. DISCUSSION

From the presented data on magnetic properties of thin orthoferrite films and single crystals, it is evident that the thin-film properties are highly affected by the epitaxial lattice strain and hence very different compared to single-crystal data. Most noticeable is the significant shift in T_{SR} , the very broad SR, or its complete suppression during FC measurements. The latter observation is an indication that Γ_4 is the preferred magnetic space group also supported by a FM hysteresis measured between 1.6 and 390 K.

When comparing the changes in film lattice parameter for all three directions with the pressure-induced changes for a single crystal, the observed maximum changes for the lattice parameters would correspond to 12 kbar for the [100], 15 kbar for the [010], and 16.7 kbar for the [001] direction. This is clearly more than expected for the two short axes, and considerably less for the long axis if applying the rule-of-thumb criteria of 1% lattice mismatch corresponding to 10 kbar (1 GPa) epitaxial strain. Overall, these nominal pressure values are closer to a more uniform pressure distribution in the unit cell justifying the comparative approach studying magnetic properties of a single crystal under hydrostatic, uniform He pressure.

How a small perturbation in the lattice parameters of the $DyFeO_3$ unit cell can lead to noticeable changes in its magnetic properties has already been reported for single-crystal and powder samples [7]. The increase in T_{SR} with the amount of compressive epitaxial strain roughly corresponds to the compressive strain utilized in uniaxial pressure experiments on $DyFeO_3$ single crystals where a change in T_{SR} of 2 K/kbar was measured. Uniaxial measurements have the benefit when measuring materials properties in one specific direction that their pressure-dependent changes will be reflected correctly. In films we typically have anisotropic strain and hence measure a mixture representative of the properties of the different

crystallographic directions. Comparing the observed values of T_{SR} with the changes in lattice parameters, we would expect to observe a minimum change on T_{SR} of +20 K and up to 40 K based on the nominal pressure values. The observed window for T_{SR} for the different films fits well to the expected temperature interval. Whereas the Morin transition along [001] remains sharp with increasing pressure for a single-crystal SR, for films along [001] it is relatively broad (Fig. 2). This leads to the conclusion that the broadening of the SRT is the result of the anisotropic strain in these films.

Another obvious difference between single-crystal and thin-film properties is the presence of a FM hysteresis loop in $M(H)$ measurements between 1.6 and 390 K along [001]. For a single crystal, the FM hysteresis closes at T_{SR} , signaling the change from Γ_4 to Γ_1 . This does not happen in films and confirms that a Γ_4 -to- Γ_1 transition does not occur in our films as a result of strain. In addition, a double hysteresis loop originated by the coupling between the Fe and Dy spins has been observed along [100] and [001]; the probable origin of the DS hysteresis in $LuFeO_3$ thin films as a single spin system is biaxial magnetic anisotropic strain in a unit cell [38–41], giving rise to a stronger Fe-O octahedra tilting and hence a canting along both in-plane directions. The DS hysteresis is clearly more pronounced in the thicker film where strain along [100] changes from compressive to tensile biaxial anisotropy alike.

The presence of the DS hysteresis in $DyFeO_3$ also reveals a large coercive field H_{C2} of up to 1 T. It is, however, smaller than the critical field of 2.3 T needed to induce ferroelectricity in bulk. The combination of growth-induced “pressure” and H_{C2} is sufficient to drive a polar state in $DyFeO_3$ [22]. It is at present not clear if the polar state can be maintained sufficiently well in order to have ferroelectricity reliably or if depolarization effects come into play. The orientation dependence of H_{C2} is also suggestive of [100] probably being the polar axis instead of [001] as reported for single crystals.

V. CONCLUSIONS

We have studied structural and magnetic properties of compressively strained orthorhombic (010)-oriented $DyFeO_3$ and $LuFeO_3$ thin films grown on (010)-oriented $YAlO_3$ and compared the results to the pressure dependence of the (031) magnetic Bragg peak for a $DyFeO_3$ single crystal under uniaxial strain. (010) $DyFeO_3$ thin films grow coherent up to 40 nm, with some lattice relaxation and a smaller unit cell volume than unstrained $DyFeO_3$. Thicker films relax towards bulk lattice values with the net unit cell volume larger than the bulk. For those films strain is mostly tensile for all directions, for films thinner than 40 nm compressive along [100] and [001] and tensile along [010]. For $LuFeO_3$, strain states are similar to $DyFeO_3$ for very thin films. For both materials, this is indicative of a Poisson ratio <0.5 when grown as a thin film.

Shifting T_{SR} for $DyFeO_3$ films by more than 20 K to higher temperatures or even completely suppressing the spin reorientation for thinner films (<40 nm) with an applied magnetic field shows the presence of the Γ_4 phase. This is substantiated by measuring double-step hysteresis loops

in the whole measured temperature range above $T_{N,Dy}$ and the presence of an induced magnetically ordered Dy lattice. As Dy orders antiferromagnetically, the DS hysteresis loops disappear and an exchange bias effect has been observed instead.

The magnetic field at which the DS hysteresis occurs is of the order of 1 T and could be large enough to drive the unit cell polar. Dy^{3+} is magnetically active along [100] and [001] with the preference in the [100] direction. Since an ordering of the Fe lattice induces ordering in the Dy lattice and ferroelectricity in bulk is linked with a ferromagnetically ordered Dy lattice in the Γ_4 phase, it is expected to observe ferroelectricity along the [100] direction in $DyFeO_3$ thin films between $T_{N,Dy}$ and 390 K. For $LuFeO_3$ we also observe DS hysteresis loops along [100] due to a strain-induced magnetic

anisotropy. It is therefore likely to measure a polar response at room temperature and above along the a direction as predicted by theory. Polarization measurements are required to show if magnetic anisotropy for both materials is the mechanism to induce ferroelectricity, which would then be a generic mechanism for this class of materials.

ACKNOWLEDGMENTS

This work was supported by the Swiss National Science Foundation (Project No. 200020_169393) and the Paul Scherrer Institute. We also would like to acknowledge the help of V. Ukleev and D. Singh with single-crystal neutron measurements on the Morpheus beam line, and V. Y. Pomjakushin for discussions about symmetry groups.

-
- [1] R. L. White, Review of recent work on the magnetic and spectroscopic properties of the rare-earth orthoferrites, *J. Appl. Phys.* **40**, 1061 (1969).
- [2] E. Bousquet and A. Cano, Non-collinear magnetism in multiferroic perovskites, *J. Phys. Condens. Matter* **28**, 123001 (2016).
- [3] T. Nakajima, Y. Tokunaga, Y. Taguchi, Y. Tokura, and T. H. Arima, Piezomagnetolectric effect of spin origin in dysprosium orthoferrite, *Phys. Rev. Lett.* **115**, 197205 (2015).
- [4] Y. Tokunaga, S. Iguchi, T. Arima, and Y. Tokura, Magnetic-field-induced ferroelectric state in $DyFeO_3$, *Phys. Rev. Lett.* **101**, 097205 (2008).
- [5] S. Cao, L. Chen, W. Zhao, K. Xu, G. Wang, Y. Yang, B. Kang, H. Zhao, P. Chen, A. Stroppa, R.-K. Zheng, J. Zhang, W. Ren, J. Íñiguez, and L. Bellaiche, Tuning the weak ferromagnetic states in dysprosium orthoferrite, *Sci. Rep.* **6**, 37529 (2016).
- [6] Z. Y. Zhao, X. Zhao, H. D. Zhou, F. B. Zhang, Q. J. Li, C. Fan, X. F. Sun, and X. G. Li, Ground state and magnetic phase transitions of orthoferrite $DyFeO_3$, *Phys. Rev. B* **89**, 224405 (2014).
- [7] B. Biswas, V. F. Michel, Ø. S. Fjellvåg, G. Bimashofer, M. Döbeli, M. Jambor, L. Keller, E. Müller, V. Ukleev, E. V. Pomjakushina, D. Singh, U. Stuhr, C. A. F. Vaz, T. Lippert, and C. W. Schneider, Role of Dy on the magnetic properties of orthorhombic $DyFeO_3$, *Phys. Rev. Mater.* **6**, 074401 (2022).
- [8] H. J. Zhao, W. Ren, Y. Yang, X. M. Chen, and L. Bellaiche, Effect of chemical and hydrostatic pressures on structural and magnetic properties of rare-earth orthoferrites: A first-principles study, *J. Phys. Condens. Matter* **25**, 466002 (2013).
- [9] Z. Hong Jian, Y. Yurong, R. Wei, M. Ai-Jie, C. Xiang Ming, and B. Laurent, Creating multiferroics with large tunable electrical polarization from paraelectric rare-earth orthoferrites, *J. Phys. Condens. Matter* **26**, 472201 (2014).
- [10] S. Dhole, A. Chen, W. Nie, B. Park, and Q. Jia, Strain engineering: A pathway for tunable functionalities of perovskite metal oxide films, *Nanomaterials* **12**, 835 (2022).
- [11] T. Tiittanen and M. Karppinen, Structure evolution upon chemical and physical pressure in $(Sr_{1-x}Ba_x)_2FeSbO_6$, *J. Solid State Chem.* **246**, 245 (2017).
- [12] R. S. Liu, C. H. Shen, S. F. Hu, and J. M. Chen, Chemical pressure control of Curie temperature in $La_{0.6}(Ba_{0.4-x}Ca_x)MnO_3$, *Mater. Chem. Phys.* **75**, 26 (2002).
- [13] F. Mumtaz, S. Nasir, G. H. Jaffari, and S. I. Shah, Chemical pressure exerted by rare earth substitution in $BiFeO_3$: Effect on crystal symmetry, band structure and magnetism, *J. Alloys Compd.* **876**, 160178 (2021).
- [14] S. Ishiwata, Y. Kaneko, Y. Tokunaga, Y. Taguchi, T. H. Arima, and Y. Tokura, Perovskite manganites hosting versatile multiferroic phases with symmetric and antisymmetric exchange strictions, *Phys. Rev. B* **81**, 100411(R) (2010).
- [15] D. G. Schlom, L.-Q. Chen, C. J. Fennie, V. Gopalan, D. A. Muller, X. Pan, R. Ramesh, and R. Uecker, Elastic strain engineering of ferroic oxides, *MRS Bull.* **39**, 118 (2014).
- [16] K. J. Choi, M. Biegalski, Y. L. Li, A. Sharan, J. Schubert, R. Uecker, P. Reiche, Y. B. Chen, X. Q. Pan, V. Gopalan, L. Q. Chen, D. G. Schlom, and C. B. Eom, Enhancement of ferroelectricity in strained $BaTiO_3$ thin films, *Science* **306**, 1005 (2004).
- [17] J. H. Haeni, P. Irvin, W. Chang, R. Uecker, P. Reiche, Y. L. Li, S. Choudhury, W. Tian, M. E. Hawley, B. Craigo, A. K. Tagantsev, X. Q. Pan, S. K. Streiffer, L. Q. Chen, S. W. Kirchoefer, J. Levy, and D. G. Schlom, Room-temperature ferroelectricity in strained $SrTiO_3$, *Nature (London)* **430**, 758 (2004).
- [18] D. Sando, Strain and orientation engineering in ABO_3 perovskite oxide thin films, *J. Phys. Condens. Matter* **34**, 153001 (2022).
- [19] P. E. Janolin, A. S. Anokhin, Z. Gui, V. M. Mukhortov, Y. I. Golovko, N. Guiblin, S. Ravy, M. El Marssi, Y. I. Yuzyuk, L. Bellaiche, and B. Dkhil, Strain engineering of perovskite thin films using a single substrate, *J. Phys. Condens. Matter* **26**, 292201 (2014).
- [20] S. Tamulevičius, Stress and strain in the vacuum deposited thin films, *Vacuum* **51**, 127 (1998).
- [21] F. K. Chiang, M. W. Chu, F. C. Chou, H. T. Jeng, H. S. Sheu, F. R. Chen, and C. H. Chen, Effect of Jahn-Teller distortion on magnetic ordering in $Dy(Fe,Mn)O_3$ perovskites, *Phys. Rev. B* **83**, 245105 (2011).
- [22] B. Biswas, Strain-induced magneto-electric properties of epitaxial (010) o - $DyFeO_3$ thin films, *Laboratory of Anorganic Chemistry* (ETH Zurich, Zurich, 2021).
- [23] U. Stuhr, B. Roessli, S. Gvasaliya, H. M. Rønnow, U. Filges, D. Graf, A. Bollhalder, D. Hohl, R. Bürge, M. Schild, L. Holitzner, C. Kaegi, P. Keller, and T. Mühlebach, The thermal triple-axis-spectrometer EIGER at the continuous spallation

- source SINO, *Nucl. Instrum. Methods. Phys. Res. A* **853**, 16 (2017).
- [24] N. Aso, Y. Uwatoko, H. Kimura, Y. Noda, Y. Yoshida, S.-I. Ikeda, and S. Katano, A uniaxial pressure cell for neutron diffraction investigation and its use in studying the single-crystalline $\text{Sr}_3\text{Ru}_2\text{O}_7$ compound, *J. Phys. Condens. Matter* **17**, S3025 (2005).
- [25] W. F. Kuhs, E. Hensel, and H. Bartels, Gas pressure cells for elastic and inelastic neutron scattering, *J. Phys. Condens. Matter* **17**, S3009 (2005).
- [26] J. Paureau and C. Vettier, New high pressure cell for neutron scattering at very low temperatures, *Rev. Sci. Instrum.* **46**, 1484 (2008).
- [27] J. Wang, J. Liu, J. Sheng, W. Luo, F. Ye, Z. Zhao, X. Sun, S. A. Danilkin, G. Deng, and W. Bao, Simultaneous occurrence of multiferroism and short-range magnetic order in DyFeO_3 , *Phys. Rev. B* **93**, 140403(R) (2016).
- [28] Y.-J. Ke, X.-Q. Zhang, H. Ge, Y. Ma, and Z.-H. Cheng, Low field induced giant anisotropic magnetocaloric effect in DyFeO_3 single crystal, *Chin. Phys. B* **24**, 037501 (2015).
- [29] R. Vilarinho, P. Bouvier, M. Guennou, I. Peral, M. C. Weber, P. Tavares, M. Mihalik, M. Mihalik, G. Garbarino, M. Mezouar, J. Kreisel, A. Almeida, and J. A. Moreira, Crossover in the pressure evolution of elementary distortions in $R\text{FeO}_3$ perovskites and its impact on their phase transition, *Phys. Rev. B* **99**, 064109 (2019).
- [30] C. W. Searle, On the pressure dependence of the low-temperature transition in hematite, *Phys. Lett. A* **25**, 256 (1967).
- [31] I. N. Goncharenko, J. M. Mignot, G. Andre, O. A. Lavrova, I. Mirebeau, and V. A. Somenkov, Neutron diffraction studies of magnetic structure and phase transitions at very high pressures, *High Pressure Res.* **14**, 41 (1995).
- [32] See Supplemental Material at <http://link.aps.org/supplemental/10.1103/PhysRevMaterials.8.084404> for additional information to magnetic moment vs film thickness along [001], and single crystal $M(T)$ data.
- [33] Y. Suzuki, Epitaxial spinel ferrite thin films, *Annu. Rev. Mater. Res.* **31**, 265 (2001).
- [34] A. N. Bogdanov, A. V. Zhuravlev, and U. K. Rößler, Spin-flop transition in uniaxial antiferromagnets: Magnetic phases, reorientation effects, and multidomain states, *Phys. Rev. B* **75**, 094425 (2007).
- [35] U. K. Rößler and A. N. Bogdanov, Magnetic states and reorientation transitions in antiferromagnetic superlattices, *Phys. Rev. B* **69**, 094405 (2004).
- [36] J. S. Kim, C. I. Cheon, C. H. Lee, and P. W. Jang, Weak ferromagnetism in the ferroelectric BiFeO_3 - ReFeO_3 - BaTiO_3 solid solutions ($\text{Re} = \text{Dy, La}$), *J. Appl. Phys.* **96**, 468 (2004).
- [37] K. N. Martin, K. Wang, G. J. Bowden, P. A. J. de Groot, J. P. Zimmermann, H. Fangohr, and R. C. C. Ward, Spin-flop transition driven by exchange springs in $\text{ErFe}_2/\text{YFe}_2$ multilayers, *J. Appl. Phys.* **101**, 09K511 (2007).
- [38] J. Shen, H. Zhao, B. Song, R. Liu, J. Du, Q. Xu, and Q. Li, Electronic structures and magnetic studies of SmFeO_3 thin films and powders, *J. Magn. Magn. Mater.* **527**, 167724 (2021).
- [39] J. Zhao, S. Liu, W. Zhang, Z. Liu, and Z. Liu, Structural and magnetic properties of Er-doped BiFeO_3 nanoparticles, *J. Nanopart. Res.* **15**, 1969 (2013).
- [40] X. Xu and W. Wang, Multiferroic hexagonal ferrites ($h\text{-RFeO}_3$, $R = \text{Y, Dy-Lu}$): A brief experimental review, *Mod. Phys. Lett. B* **28**, 1430008 (2014).
- [41] S. G. Titova, E. V. Sterkhov, and S. A. Uporov, Crystal structure and magnetic properties of A-site substituted $\text{Nd}_{1-x}\text{Pr}_x\text{BaMn}_2\text{O}_6$ double manganite, *J. Supercond. Novel Magn.* **33**, 1899 (2020).